Stimuli-responsive Materials from Ferrocene-based Organic Small Molecule for Wearable Sensors

Ling Li, Jianyu Zhang, Chenyi Yang, Le Huang, Jun Zhang, Jie Bai, Carl Redshaw, Xing Feng, Changyong Cao,* Nengjie Huo, Jingbo Li,* Ben Zhong Tang**

((Optional Dedication))

L. Li, C. Yang, Dr. L. Huang, Dr. J. Bai, Dr. X. Feng
School of Material and Energy, Guangdong University of Technology, Guangzhou 510006, P. R. China
E-mail: hyxhn@sina.com (X. Feng)

Dr. J. Zhang, Prof. Dr. B. Z. Tang
Department of Chemistry, The Hong Kong Branch of Chinese National Engineering Research Center for Tissue Restoration and Reconstruction, Institute for Advanced Study and Department of Chemical and Biological Engineering, The Hong Kong University of Science and Technology, Clear Water Bay, Kowloon, Hong Kong, China
E-mail: tangbenz@ust.hk (B. Z. Tang)

Prof. Dr. J. Zhang
School of Materials and Chemical Engineering, Anhui Jianzhu University, Hefei, 230601, People's Republic of China

Prof. Dr. C. Redshaw
Department of Chemistry, University of Hull, Cottingham Road, Hull, Yorkshire HU6 7RX, UK.

Prof. Dr. C. Cao
Laboratory for Soft Machines & Electronics, Departments of Mechanical Engineering, Electrical and Computer Engineering, Michigan State University, East Lansing 48824, MI,
E-mail: ccao@msu.edu (C.Y. Cao)

L. Li, Prof. Dr. N. Huo, Prof. Dr. J. Li
Institute of Semiconductors, South China Normal University, Guangzhou 510631, P. R. China.
E-mail: jbli@semi.ac.cn (J. B. Li)

Keywords: piezoelectricity, aggregation-induced emission, organic small molecules, polarizability, wearable devices

Abstract: Stimuli-responsive crystals capable of energy conversion have emerged as promising materials for smart sensors, actuators, wearable devices, and robotics. Here we report a novel ferrocene-based organic molecule crystal (**Fc-Cz**) that possesses anisotropic piezoelectric, optical, and mechanical properties. We demonstrate that the new crystal **Fc-Cz** can be utilized as an ultrasensitive piezoelectric material in fabricating strain sensors and energy harvesters. The flexible sensor made of crystal **Fc-Cz** can detect small strains/deformations and motions with a fast response speed. Analysis based on density functional theory (DFT) indicates that an external pressure can affect the dipole moment by changing the molecular configuration of the asymmetric single crystal **Fc-Cz** at the crystalline state, leading to a change of polarity, thereby an enhanced dielectric constant. This work has demonstrated a new artificial organic small molecule for high-performance tactile sensors, indicating its great potential for developing low-cost flexible wearable sensors and energy harvesters.

1. Introduction

Stimuli-responsive materials have been widely used for actuators and sensors in advacned robotics,[1] structural health monitoring devices,[2] and human machine interfaces,[3] due to their high sensitivity and fast response to the variation of external environmental conditions (e.g., pressure, temperature, and pH).[4, 5] As one common smart material, piezoelectric materials are utilized to develop pressure sensors of smart wearables, and much effort is focused on how to improve the sensitiveity, response speed, and operation stability through modifying material constitution and microstructures. Piezoelectric effect is atributed to the polarization charges of piezoelectric materials under mechanical deformations along the polarization direction in the non-centrosymmetric materials.[6] Many piezoelctric materials have been used for constructing E-skins, including carbon-based materials (carbon

nanotubes,[7] graphene[8]), polymer nanofibers,[9] perovskite,[10] 2D layered materials (such as α-In_2Se_3),[11-13] inorganic complexes[14, 15] as well as bio-organic and natural biomaterials.[16]

Compared with traditional inorganic piezoelectric materials, synthesized small organic molecules may be better cadidates for novel piezoelectric materials because they i) possess tunable molecular frameworks, ii) adopt precise molecular structures with unique molecular conformations, and iii) exhibit controllable molecular packing in solid state. Moreover, theoretical calculations have revealed that the presence of hydrogen bonding plays a significant role in achieving a larger piezo-response.[17] Organic materials with numerous hydrogen bonds in their molecular packing can be efficient organic piezo-response materials for enhacing their piezoelectric properties.

Some bio-organic and natural biomaterials such as amino acids/proteins possess relatively weak piezoelectric effects and can be used for nanoelectronics.[18,19] For example, Thompson and coworkers utilized the piezoelectric properties of glycine polymorphs for biopiezoelectric sensing and energy harvesting.[20] Kholkin *et al*. observed that self-assembled diphenylalanine peptide nanotubes (PNTs) exhibited strong anisotropic piezoelectricity with the orientation of polarization along the axis of the tube.[21] However, developing unique molecular architectures with strong piezoelectricity based on man-made organic molecules remains challenging and rare solutions are reported.

Ferrocene, $Fe(C_5H_5)_2$, is an aromatic hydrocarbon compound with a sandwiched structure. The Fe atom between the two parallel cyclopentadienyl (Cp) rings exhibits an intriguing magnetic property and shows promise in electron transport and spin filtering.[22, 23] Thus, various ferrocene-based complexes have been investigated for organic photoelectric-magnetic functional materials. On the other hand, due to the high-energy lone pair at the Fe atom in the ferrocene unit, ferrocene-containing compounds exhibit

weak/non-emission through intramolecular photoinduced electron transfer (PET) reactions, which may be an excellent "turn-on" probe to detect the metal cation and anion by lowing the energy of the lone pair.[24]

Aggregation-induced emission (AIE) is a new phenonma in which a series of twisted luminogens exhibited non-luminescent in solution but enhanced fluorescence intensity in solid state.[25-27] Cyanostilbene derivatives are widely used to develop new AIE luminogens, and these organic molecules exhibit high efficiency in mechanoluminescence (ML) and luminescence photoluminescence (PL) at solid state. Moreover, the conformation of the packing mode significantly affects the ML behavior of AIE.[28-30] However, it is not clear how AIE luminogens interact with organic photoelectric-magnetic materials.

Here, a new small organic molecule (**Fc-Cz**) is designed and readily synthesized by combining the cyanostilbene and the ferrocene motifs via Knoevenagel reaction. The crystal packing, thermal behaviors, photophysical properties, and electrical properties of the **Fc-Cz** are investigated in detail. Experimental results show that the crystalline **Fc-Cz** has strong anisotropic piezoelectricity under external stimuli, achiving a maximum peak current of 580 pA. Flexible tactile sensors are developed based on the advanced piezoelectric property of **Fc-Cz**, demonstrating its good sensitivity and fast response speed in detecting human motions.

2. Results and Discussion

2.1. Synthesis and characterization of Fc-Cz crystal

Figure 1A illustrates the synthetic route of the target compound (**Fc-Cz**) in 80% yield through a Knoevenagel reaction between ferrocene carboxaldehyde and 2-(4'-(8a,9a-dihydro-9H-carbazol-9-yl)-[1,10-biphenyl]-4-yl)acetonitrile (**1**) [31] in dry ethanol. The molecular structure **Fc-Cz** was fully characterized by $^{1}H/^{13}C$ NMR spectra, high

resolution mass spectra (HRMS), and single crystal X-ray crystallography. **Fc-Cz** possesses excellent solubility in most common organic solvents, such as toluene, tetrahydrofuran (THF), dichloromethane, dimethyl sulfoxide (DMSO), and *N*,*N*-dimethylformamide (DMF). Therefore, a single crystal of **Fc-Cz** can be cultivated by slow evaporation of a mixture of hexane and chloroform. The molecular structure and crystal pattern (**Figure 1B**) were confirmed by X-ray crystallography. The basic crystallographic data and structure refinement parameters are summarized in **Table S1**.

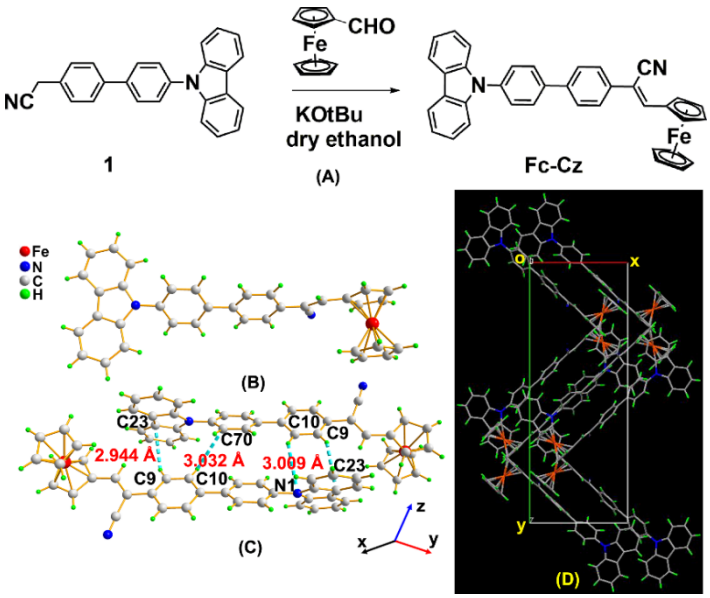

Figure 1. Synthesis and characterization of Fc-Cz. (A) Synthetic route for the compound Fc-Cz, (B) Crystal structure of Fc-Cz, (C) Packing structure adopted via C-H π interactions, (D) Packing structure of Fc-Cz along z-axis view.

The single crystal **Fc-Cz** is monoclinic, space group P2(1)/c. The asymmetric unit contains one molecule, and the molecule adopts a twisted conformation between the carbazole and two phenyl moieties with a twist angle of 61.73 ° and 78.10 °, respectively. The ferrocene unit is almost parallel with the carbazole unit, and the compound **Fc-Cz** adopts a head-to-tail packing pattern through several C-H···π interactions with distances in the range of 2.944 ~ 3.031 Å. The crystals form an ordered tight crystal-state packing along the *a*-axis and the *c*-axis directed by weak C-H···π interactions (**Figure 1C-D**), while adopt a loose packing

pattern with unconspicuous overlaps and weak intermolecular interactions along the *b*-axis.[32] Moreover, **Fc-Cz** adopts a herringbone pattern along the *b*-axis (**Figure S3-2**), and this packing contributes to the improvment of the mechanical properties of the crystal.[33]

2.2. UV-Vis measurements of Fc-Cz

The UV-visible absorption spectra of compound **Fc-Cz** were respectively measured in a THF solution (10^{-5} M) and in the solid state. As shown in Figure S4-1, the UV spectra exhibited two strong absorption peaks at 278 nm and 341 nm, respectively, and a weak absorption band in the range of 430-600 nm, which was assigned to the metal-to-ligand charge transfer (MLCT) transition. The compound **Fc-Cz** exhibited a weak blue emission with a maximum emission peak at 397 nm in solution. Although the crystal **Fc-Cz** did not emit any fluorescene in solid state using a fluorescence spectrophotometry (λ_{ex} = 291 nm), a weak, wide emission peak in the range from 350 to 600 nm was observed under the 325 nm laser irradiation (Figure S4). This may be attrributed to the synergic effects of the strong twisted intramolecular charge transfer (TICT) effect and the strong PET from the ferrocene to the phenyl-phenyl carbazole fragment.

2.3. Polarization-dependent photoluminescence (PL) spectrum of Fc-Cz crystal

The molecule **Fc-Cz** crystallizes in the monoclinic $P2_1/c$ space group, and its low symmetry in a unit cell indicates that the anisotropic excitons will dominate the excitonic state and enhance the excitonic effects.[34, 35] Thus, polarization-dependent photoluminescence (PL) is performed to understand the anisotropic optical properties *via* angle-resolved polarized photoluminescence spectroscopy (ARPPS) (**Figure 2A**).[36] A high-quality, single rod-like crystal **Fc-Cz** (15 × 50 μm) is transfered to a SiO_2/Si substrate, the orientation-dependent photoluminescence property is measured under a 532 nm excitation laser (**Figure 2B**). During

the measurements, the rotation angle (θ) from 0° to 360° (every 10°) of the sample is operated in a clockwise direction. The PL diagram is presented in **Figure 2C**.

In particular, a strong and intensive PL peak at 581 nm is observed under un-polarization. When the excitation laser polarization direction (i.e., the angle φ between the incident light and PL detector) is fixed at 0°, as the rotation angle(θ) increases from 0° to 180° (along the *z*-axis), the PL intensity reduces from 458 au to 76 au (θ = 0 ° ~ 90 °), then increases to 409 au (θ = 90° ~ 180°). The maximum/minimum related intensity ratio (I_{max}/I_{min}) is up to 6.0 and the polarization ratio $\rho_{PL}=(I_{max} - I_{min})/(I_{max} + I_{min})$ is *ca*. 0.72. It is obvious that the anisotropy has a significant effect on the PL intensity, as shown in the two-lobed polar plot (**Figure 2D-E**). When the excitation laser is polarized along the direction φ = 45°, the crystal **Fc-Cz** exhibits a similar polarization PL behavior with a polarization ratio ρ_{PL} of 0.63. The polar plot exhibits a four-leaf clover structure when the polarization orientation of excitation laser increrases to φ = 90°. The polarization PL intensity is generally related to the angle-dependant near-gap excitons.[34,35] The polar plot indicates that the direct recombination of excitons is mainly concentrated along the *z*-axis (001 plane) of crystal **Fc-Cz**. For comparison, the above-mentioned polarization resolved spectra with φ = 0° is repeatedly measured for similar polarization PL behaviors at extra two points (**Figure S4-6**, point B and C) of the same crystal sample, indicating that the same molecular orientation exists in the **Fc-Cz** crystal along the *z*-axis (001) planes (**Figure S4-6**). The above ARPPS results confirm that the crystal **Fc-Cz** has well-defined anisotropic-dependent optical properties.

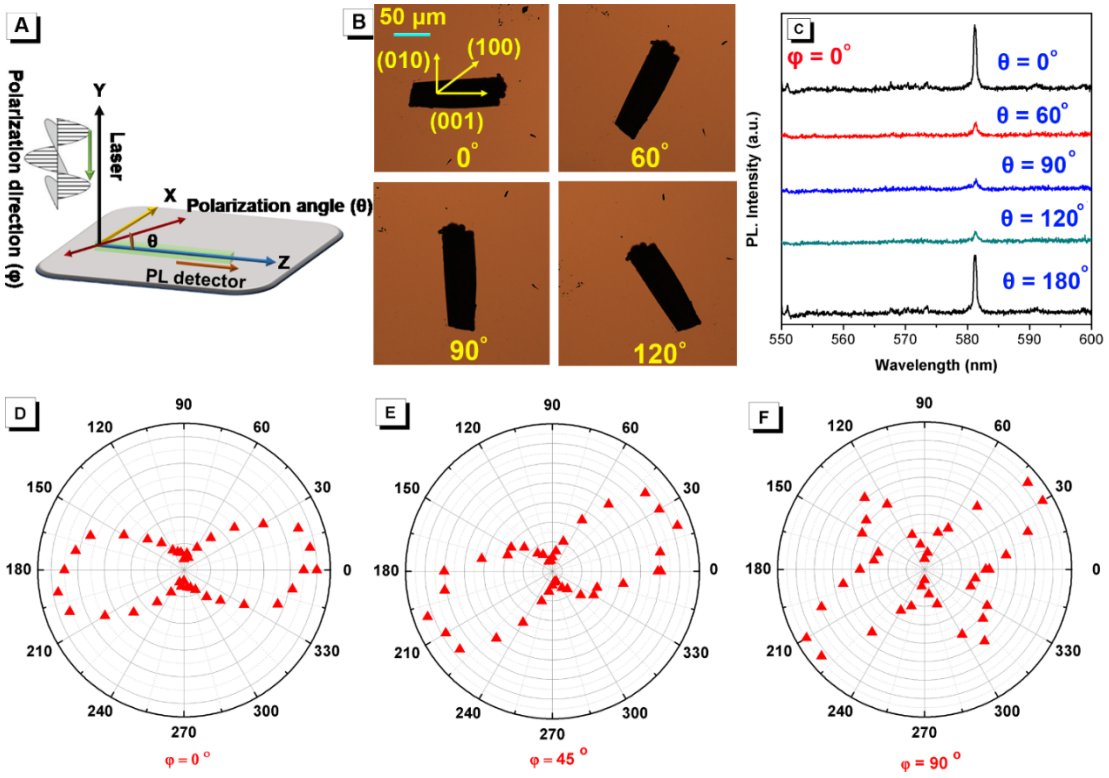

Figure 2. Polarization-dependent photoluminescence (PL) measurements. (A) Schematic of the configuration for PL measurement. (B) Photographs of a crystal **Fc-Cz** sample on a Si/SiO_2 substrate with polarization orientations. (C) PL spectra obtained at different polarization angles. (D-F) Angular-dependent PL of the maximum intensity of peak at 583 nm when φ= 0°, 45°, and 90°.

2.4. Piezoelectric properties of Fc-Cz crystal

The transport properties of organic meterials such as charge carrier mobility have significnt effect on the performance of organic semiconducting devices.[12,13,36-38] In our study, we fabricat a flexible piezoelectric sensor using a metal–organic semiconductor–metal (MOM) structure on a polyimide (PI) substrate. Based on the crystal structure, the compound **Fc-Cz** interacts with one another by a series of C-H···πinteraction and the van der Waals force, and exhibits good mechanical performance, with an average Young's modulus of 3.23 Gpa. In the fabrication of the designed pressure sensor, silver paste is used for the electrodes, and the rod-like crystal **Fc-Cz** is aligned along the *z*-axis (001-plane) to connect the two metal electrodes (**Figure 3A**). The channel length of the device was about *ca*. 25 μm (**Figure S7-1**). **Figure 3B** shows the induced piezoelectric current as a fucntion of the applied strain under a bending load on the device. As shown in **Figure 3C-D** and **Figure S6-4**, when the pressure sensor is subjected to a cyclic strain (bending-releasing) for one hundred cycles, the crystal **Fc-Cz** shows a stable piezoelectric signal. Furthermore, we found that the piezoelectric signal

output (I_{ds}) has slightly changed when the strain changing is less than 0.25%-0.3%, and the bent ferrocene will not only generate a piezoelectric signal, but also the piezoelectric signal under applied strain, the combined effect of the piezoelectric effect and the piezoresistive effect makes the piezoelectric signal approximately constant. The data points we tested are piezoelectric signals with obvious changes. the nonlinear relationship between the piezoelectric signal and strain of the crystal **Fc-Cz** was clarified by a mathematical fitting formula $y=a*x^b$, where x is strain and y is the voltage signal. Since the piezoelectric current and voltage signal as a fucntion of the applied strain are different, the values of a and b are also different. The voltage signal (current signal) along the z-axis is a=38, b=3 (a=82, b=4). The voltage signal (current signal) along the x-axis is a=1, b=2 (a=49, b=3) (Figure S6-8).

When the applied strain is along the *z*-axis of the crystal **Fc-Cz**, a negative current output is rapidly generated, and a positive output was observed as the strain is removed. The response time is <40 ms. As shown in **Table S3**, the piezoelectric sensitivity of crystal **Fc-Cz** can be as high as 350 pA/ε (up to 94 mV/ε) when the strain is 1.7%, which is superior to that of most 2D materials and has a larger working strain range (0.2%~1.7% strain). **Figure 3** and **Figure S6** exhibit the dynamic piezoelectric signals as a function of applied strain along different directions. The dynamic piezoelectric signals are enhanced as the applied strain increases from 0.2 % to 1.7 % along the *z*-axis (001) (**Figure 3C**, **Figure S6-2 and Figure S6-3**). However, under the same strain, the maximum peak current (or voltage) is *ca*. 2-fold of that along the *z*-axis (001) compared to *x*-axis (100). This is attributed to the anisotropy of the crystal **Fc-Cz**, in agreement with the previous reports for 2D layered materials.[38] When the applied strain is up to 1.7% along the *z*-axis, the maximum peak current (or voltage) reaches > 580 pA (or 140 mV), which is about 80 times (or 23 times) higher than the induced current at a strain of 0.7%. This indicates that the piezoelectric perfromance of the crystal **Fc-Cz** is better than other reported materials such as two-dimensional (2D) ultrathin semiconductors (GaS, GaSe, In_2Se_3, MoS_2, $MoSe_2$, and graphene-based composites[12-14, 36-39]), leading to possible ultrasensitive piezoelectric devices (Table S3).

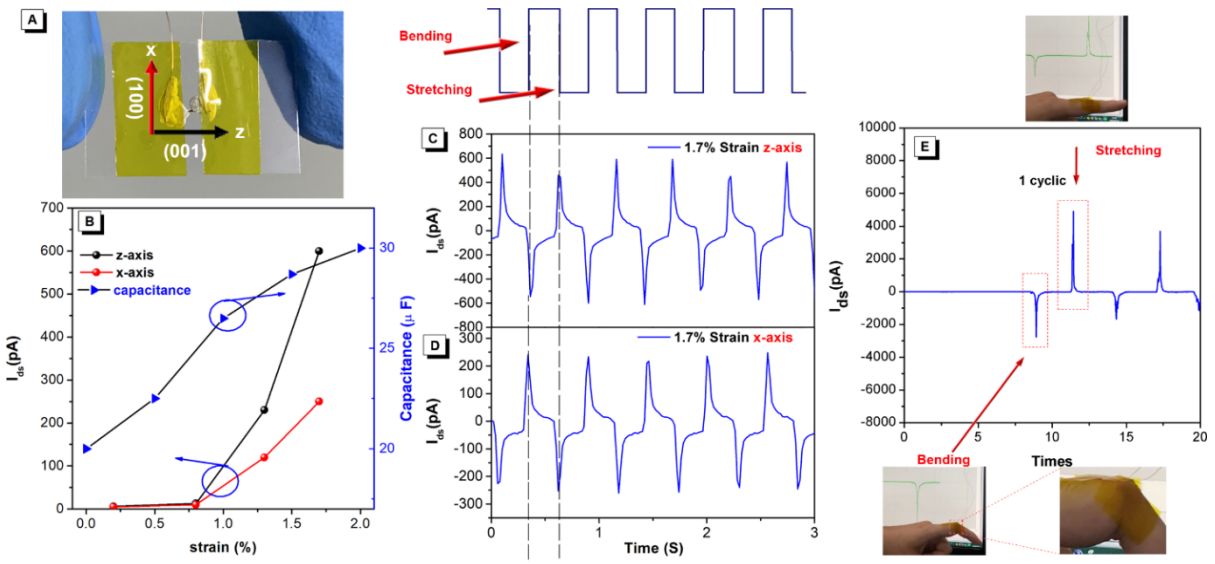

Figure 3. Piezoelectric performance of the Fc-Cz for ferrocene-based small organic molecule nanogenerators. (A) The photograph of the flexible piezoelectric nanogenerators. (B) The relationship between electrical output (capacitance) and strain. (C-D) Short-circuit current response of the ferrocene-based small organic molecule nanogenerator under applied periodic strains along the *z*- and *x*-axes. (E) Demonstration of a flexible wearable device worn on the forefinger for detecting pulse waves. Insert: the wrist wearing experiments under stretching-bending motion states in a cycle.

On the contrary, in the absence of ferrocene units, the compound 2-(4'-(8a,9a-dihydro-9H-carbazol-9-yl)-[1,10-biphenyl]-4-yl)acetonitrile (**1**) shows a weaker piezoelectric performance than the **Fc-Cz** crystal. Although a very small electronic signal is also detected under large strains, the compound **1** demonstrates to be brittle and generates a low current peak (~38 pA) under a strain of 1.3% (**Figure S6-6**). Thus, the new ferrocene-based organic small molecular semiconductor is a superior candidate for developing flexible piezoelectric generators in broad applications such as E-skin and self-powered sensening devices.

We also fabricate a wearable tactile sensor by transferring a thin **Fc-Cz** film onto a PDMS substrate to monitor human motions. As shown in **Figure 3E**, the tactile sensor worn on the forefinger is encapsulated by a polyimide film. When the forefinger performs a cyclic bending-unbending motion, the induced piezoelectric current changes with the variation of the

bending angle. It is demonstrated that a maximum current of ~3600 pA can be generated when the finger bending angle reaches ~70°. The flexible tactile sensor also exhibits good stability, high sensitivity, and excellent repetitivity in detecting the continuous motions of a human hand (see Movie 1 in **SI**). Therefore, this small molecular organic semiconductor **Fc-Cz** has the great potential for developing future wearable devices.

2.5. The relationship between piezoelectricity, dielectric and polarizability

Theortically, the external forces play a key role in the flexible organic molecular pattern in the crystal/aggregation state[40], leading to some macroscopic photophysical or chemical behaviors like mechanoluminescence.[41-43] It is measured that the capacitance of the flexible piezoelectric nanogenerator can be enhanced from 6 to 30 μF as the applied strain increases along the *x*-axis, following the trends of dynamic piezoelectric signals. The relationship between capacitance and dielectric constant can be expressed as

$$\varepsilon_r = C \cdot d / \varepsilon_0 S \quad (1)$$

where ε_r is the relative dielectric constant, C is the capacitance, ε_0 is the vacuum dielectric constant (8.854×10^{-12} F/m), and S is the area of a sample. The polarizability X is calculated by

$$X = \varepsilon_r - \varepsilon_0 \quad (2)$$

It can be rewritten as

$$X = C \cdot d / (\varepsilon_0 \cdot S) - \varepsilon_0 \quad (3)$$

Thus, the polarizability X is positively associated with the relative dielectric constant of the material. It is assumed that the relative polarizability and the dipole moment of crystal **Fc-Cz** change with the applied strain.[44] To reveal the relationship between the piezoelectricity, dielectriccity, and polarizability of crystal **Fc-Cz**, we perform density functional theory (DFT) analysis at the PBE0/def2-SVP level. Analytical frequency calculations are also performed at the same level of theory to verify that the optimized

structure is at the minimum point. The highest occupied molecular orbital (HOMO) and the lowest unoccupied molecular orbital (LUMO) are isolated and mainly located on the carbazole unit and the diphenyl fragment, respectively. The calculated HOMO and LUMO energies are respectively–5.93 eV and -2.20 eV, and the energy gap between them is 3.73 eV (**Figure 4A**). Furthermore, the HOMO level of the compound **Fc-Cz** is confirmed to be -5.72 eV by XPS. The optical energy gap derived from the lowest energy absorption onset in the absorption spectra is 3.14 eV, therefore, the corresponding LUMO level is -2.58 eV. These results varify a good agreement between the experimental and theoretical studies.

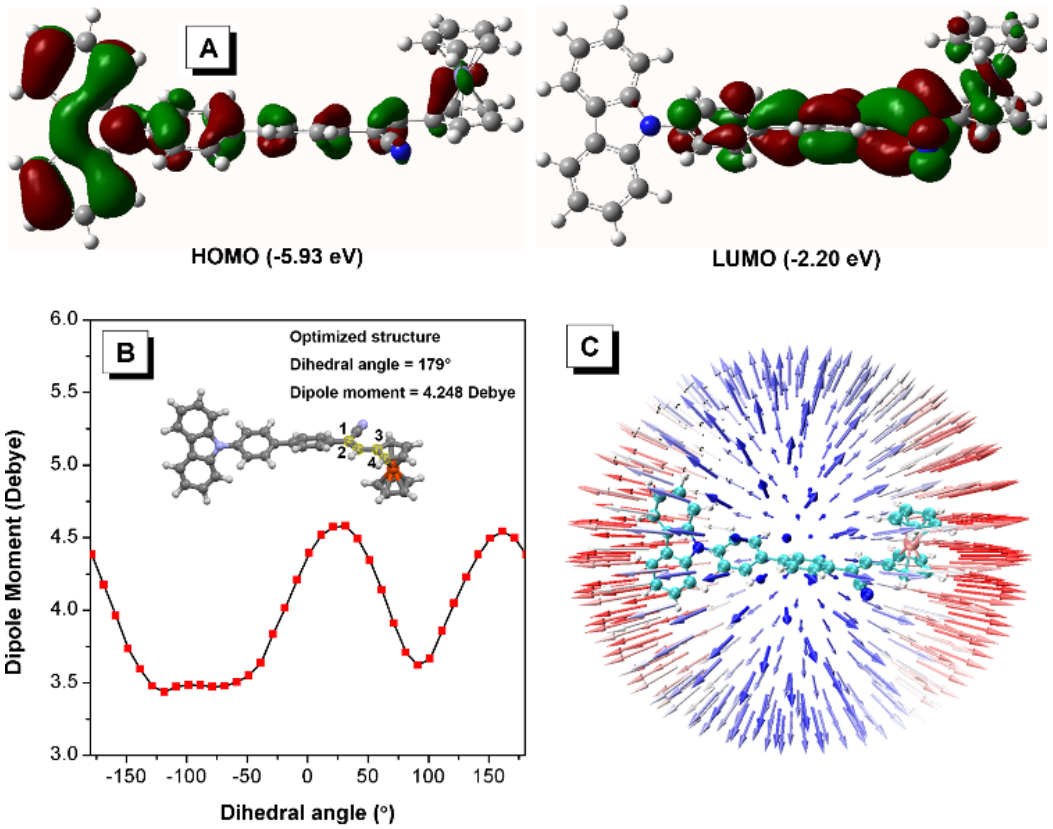

Figure 4. (A) Computed molecular orbital plots of compound **Fc-Cz**. (B) Calculated dipole moment of **Fc-Cz** with different dihedral angles (∠1-2-3-4)**. (C)** Visualization of the polarizability tensor of **Fc-Cz.** The unit sphere representation is colored with red being the largest magnitude effective dipoles and blue being the smallest magnitude effective dipoles, calculated at PBE0/def2-SVPD level, Gaussian 16 program.

Starting from the optimal structure, different structures are scanned along the ferrocene group (dihedral angle ∠1-2-3-4, as shown in **Figure 4B**) at the same level. Their dipole

moments are further evaluated at the PBE0/def2-SVPD level. The polarizability and the surface of the polarizability tensor are analyzed using the Multiwfn package and VMD software.[43, 44] The ferrocene unit is almost perpendicular to the phenyl ring at an angle of 71.7° in the optimized structure (the dihedral angle ∠1-2-3-4 = 179°), and the corresponding dipole moment is 4.248 Debye. Indeed, as the dihedral angle ∠1-2-3-4 changes in the range from 0 to 90° (or from -180° to -120°), the dipole moment decreased from 4.58 to 3.62 (or 3.50) Debye. The relatively large change of dipole with dihedral angle (large slope) indicates that the small changes of molecular comformation can greatly affect the molecular dipole moment. Furthermore, the periodic DFT calculation is further performed by a VASP code based on the X-ray single crystal structure model under a compressive strain of 5%,[45] the dipole moment of the unit cell of crystal **Fc-Cz** decreases from 3.80, 0.58, and 2.83 Debye to 3.12, 0.53, and 2.64 Debye alone a-, b- and c-axis, respectively. Thus, the periodic strain within the **Fc-Cz** device leads to the slight change of molecular configuration, thereby a relatively dynamic dipole moment fluctuation that is favorable for variational polarizability.

The 3D visualization of the first hyperpolarizability tensor can shed new light on the relationship between the piezoelectric properties and the molecular structure.[46] The visualization unit sphere indicates that the maximum second harmonic is along the *z*-axis of the molecular framework compared to the vertical direction (*y*-axis), corresponding to the (010) plane of the crystal **Fc-Cz (Figure 4C)**. On the other hand, Hirshfeld surface analysis is performed to quantify the intermolecular interaction in the crystal state, which provides a relative proportion of C···H, N···H, and H···H with intermolecular contacts at 38.9%, 8.0%, and 50.8%, respectively. The presence of the weak intermolecular interactions contributes to the enhancement of the piezo-coefficient of the organic piezoelectric material **Fc-Cz**.

3. Conclusion

In this paper, we have synthesized a a small organic molecular crystal (**Fc-Cz**) and demonstrated its high anisotropy-piezoelectric properties (~580 pA) and fast response speed (< 40 ms). Thanks to the low symmetry in material structure, the new crystal possessed orientation-dependent photoluminescence properties and exhibited a maximum polarity ratio of 0.72. The experimental and theoretical studies showed that the piezoelectricity, dielectric, and polarizability of the material have positive correlation. The flexible tactile sensor made of crystalline **Fc-Cz** exhibited good stability, high sensitivity, and good reproducibility in detecting the continuous motions of a human hand. This research provides a new candidate and possible solution for developing advanced artificial organic materials as piezoelectric materials for potential applications in E-skin, wearable devices, energy harvesting, and human–machine interaction.

4. Experimental Section

Materials Preparation. Unless otherwise stated, all reagents were purchased from commercial sources and were used without further purification. The starting material 2-(4'-(8a,9a-dihydro-9H- carbazol-9-yl)- [1,10-biphenyl]-4-yl)acetonitrile was prepared following the procedures in a previous report.[31]

Materials Characterization. ^{1}H and ^{13}C NMR spectra were recorded on a Bruker AVANCE III 600M spectrometer using chloroform-*d* solvent and tetramethylsilane as internal references. *J*-values are given in Hz. High-resolution mass spectra (HRMS) were taken on a LC/MS/MS, which consisted of a HPLC system (Ultimate 3000 RSLC, Thermo Scientific, USA) and a TSQ Endura QQQ mass spectrometer. UV-vis absorption spectra and Photoluminescence (PL) spectra were recorded on a Shimadzu UV-2600 and the Hitachi F-4700 fluorescence spectrometer. The quantum chemistry calculations were performed using the Gaussian 16W (PBE0/def2-SVPD basis set) software package. [47,48]

X-ray Crystallography. Crystallographic data for the compound was collected on a Bruker APEX 2 CCD diffractometer with graphite monochromated Mo Kα radiation (λ = 0.71073 Å) in the ω scan mode.[49,50] The structure was solved by charge flipping or direct methods algorithms and refined by full-matrix least-squares methods on F^2.[49] All esds (except the esd in the dihedral angle between two l.s. planes) were estimated using the full covariance matrix. The cell esds were considered individually in the estimation of esds in distances, angles and torsion angles. Correlations between esds in cell parameters were only used when they were defined by crystal symmetry. An approximate (isotropic) treatment of cell esds was used for estimating esds involving l.s. planes. The final cell constants were determined through global refinement of the xyz centroids of the reflections harvested from the entire data set. Structure solution and refinement were carried out using the SHELXTL-PLUS software package.[50] Data (excluding structure factors) on the structures reported here had been deposited with the Cambridge Crystallographic Data Centre with deposition numbers. CCDC 2041456 contain the supplementary crystallographic data for this paper. These data could be obtained free of charge from The Cambridge Crystallographic Data Centre via www.ccdc.cam.ac.uk/data_request/cif.

Synthesis of (Z)-2-(4'-(9H-carbazol-9-yl)-[1,1'-biphenyl]-4-yl)-3- ferrocene acrylonitrile (Fe-Cz). Ferrocene carboxaldehyde (65 mg, 0.3 mmol, 1.07 eq.), 2-(4'-(8a,9a-dihydro-9H-carbazol-9-yl)-[1,10-biphenyl]-4-yl)acetonitrile (100mg, 0.28 mmol, 1 eq.) and potassium *t*-butoxide (100 mg, 0.89 mmol, 3 eq.) were dissolved in 5 mL dry ethanol and stirred overnight under a nitrogen atmosphere. After it was cooled to room temperature, the solid obtained was filtered and washed with hexane. Then the black solid residue was recrystallized from a mixture of dichloromethane and *n*-hexane to afford the pure **Fc-Cz** (97 mg, 78%). ^{1}H NMR (600 MHz, $CDCl_3$) δ 8.17 (d, J = 6.9 Hz, 2H), 7.85 (d, J = 7.3

Hz, 2H), 7.75 (s, 4H), 7.67 (d, J = 6.6 Hz, 2H), 7.56 – 7.41 (m, 5H), 7.31 (m, 2H), 5.02 (s, 2H), 4.52 (d, J = 64.6 Hz, 2H), 4.23 (d, J = 47.8 Hz, 5H) ppm, ^{13}C NMR (151 MHz, $CDCl_3$) δ 143.3, 140.8, 140.0, 137.3, 128.4, 127.7, 127.5, 126.0, 125.7, 123.5, 120.4, 120.1, 71.8, 70.3, 69.9, 69.8. HRMS (FTMS + p ESI): m/z= calcd for $C_{37}H_{26}N_2Fe$ 553.1367 $[M+H]^+$; found 554.1442

PL measurement. A single rod-like crystal (20 μm (length) ×5μm (width) × 2 μm (height)) was transferred to the SiO_2/Si substrate. The angle-resolved polarized photoluminescence spectroscopy measurement was performed on a Photoluminescence instrument (Nost Technology Co., Ltd) with a laser source (λ_{ex} = 532 nm).

Device Fabrication. The crystal **Fc-Cz** (62 μm (length) × 13μm (width) × 25μm (height)) was transferred onto the polyimide (PI) substrate and fixed by silver pulp along *z*-axis (001 phase). The device was then annealed at 50 °C for 30 min. and the Piezoelectricity properties of the devices were measured on a linear motor and Keithley B2612A semiconductor analysis system.

Statements: The experiments involving a human research participant (L. Li) were performed in compliance with the relevant laws and institutional guidelines and approved by the ethics committee of Guangdong University of Technology. And these authors declare that no competing financial interest.

Supporting Information ((delete if not applicable))
Supporting Information is available from the Wiley Online Library or from the author.

Acknowledgements
L. Li and J. Zhang contributed equally to this work. This work was supported by the National Natural Science Foundation of China (21975054), Natural Science Foundation of Guangdong Province of China (2019A1515010925), "One Hundred Talents Program" of the Guangdong University of Technology (GDUT) (1108-220413205), Guangdong Provincial Key Laboratory of Information Photonics Technology (2020B121201011), the Pearl River Talent Recruitment Program" (2019ZT08X639), the Research Grants Council of Hong Kong (C6009-17G), and the Innovation of Technology Commission (ITC-CNERC14SC01). CR thanks the EPSRC for an Overseas Travel Grant (EP/R023816/1).

Received: ((will be filled in by the editorial staff))
Revised: ((will be filled in by the editorial staff))
Published online: ((will be filled in by the editorial staff))

References

[1] R. Tognato, A. Armiento, V. Bonfrate, R. Levato, J. Malda, M. Alini, D. Eglin, G. Giancane, T. Serra, *Adv. Funct. Mater.* **2018**, *29*, 1804647.

[2] Z. Deng, R. Yu, B. Guo, *Mater. Chem. Front.* **2021**, *5*, 2092-2123.

[3] M. Ding, L. Jing, H. Yang, C. Machnicki, X. Fu, K. Li, I. Y. Wong, P. Y. Chen, *Mater. Today Avd.* **2020**, *8*, 100088.

[4] B. Y. Lee, J. Zhang, C. Zueger, W.-J. Chung, S. Yoo, E. Wang, J. Meyer, R. Ramesh, S.-W. Lee, *Nat. Nanotechnol.* **2012**, *7*, 351-356.

[5] Z. L. Wang, J. H. Song, *Science* **2006**, *312*, 242-246.

[6] L. Li, W. Gao, H. Chen, K. Zhao, P. Wen, Y. Yang, X. Wang, Z. Wei, N. Huo, J. Li, *Adv. Electron. Mater.* **2020**, *6*, 1901441.

[7] F. Mokhtari, Z. Cheng, R. Raad, J. Xi, J. Foroughi, *J. Mater. Chem. A* **2020**, *8*, 9496-9522.

[8] M. T. Ong, E. J. Reed, *ACS Nano*, **2012**, *6*, 1387-1394.

[9] P. Snapp, C. Cho, D. Lee, M. F. Haque, S. Nam, C. Park, *Adv. Mater.* **2020**, *32*, 2004607.

[10] J. Hao, W. Li, J. Zhai, H. Chen, *Mater. Sci. Eng. R Rep*. **2019**, *135*, 1-57.

[11] C. Cui, F. Xue, W.-J. Hu, L.-J. Li, *NPJ 2D Mater. Appl*. **2018**, *2*, 18.

[12] S. A. Han, J. Lee, J. Lin, S.-W. Kim, J. H. Kim, *Nano Energy*, **2019**, *57*, 680-691.

[13] F. Xue, J. Zhang, W. Hu, W.-T. Hsu, A. Han, S.-F. Leung, J.-K. Huang, Y. Wan, S. Liu, J. Zhang, J.-H. He, W.-H. Chang, Z. L. Wang, X. Zhang, L.-J. Li, *ACS Nano*, **2018**, *12*, 4976-4983.

[14] M. Dai, Z. Wang, F. Wang, Y. Qiu, J. Zhang, C.-Y. Xu, T. Zhai, W. Cao, Y. Fu, D. Jia, Y. Zhou, P.-A. Hu, *Nano Lett.* **2019**, *19*, 5410-5416.

[15] S. Velasco-Lozano, M. Knez, F. López-Gallego, *ACS Appl. Energy Mater.* **2018**, *1*, 2032-2040.

[16] V. Bystrov, E. S. Hosseini, S. Kopyl, I. Bdikin, A. Kholkin, *J. Appl. Phys.*, **2014**, *116*, 066803-066803.

[17] A. Gagrai, V. Mundlapati, D. Sahoo, H. Satapathy, H. Biswal, *ChemistrySelect*, **2016**, *1*, 4326-4331.

[18] S. K. Ghosh, D. Mandal, *ACS Sustain. Chem. Eng.* **2017**, *5*, 8836-8843.

[19] D. Kim, S. A. Han, J. H. Kim, J.-H. Lee, S.-W. Kim, S.-W. Lee, *Adv. Mater.* **2020**, *32*, 1906989.

[20] S. Guerin, A. Stapleton, D. Chovan, R. Mouras, M. Gleeson, C. McKeown, M. R. Noor, C. Silien, F. M. F. Rhen, A. L. Kholkin, N. Liu, T. Soulimane, S. A. M. Tofail, D. Thompson, *Nat. Mater.* **2018**, *17*, 180.

[21] A. Kholkin, N. Amdursky, I. Bdikin, E. Gazit, G. Rosenman, *ACS Nano*, **2010**, *4*, 610-614.

[22] W. E. Geiger, *Organometallics*, **2007**, *26*, 5738-5765.

[23] D. Schaarschmidt, H. Lang, *Organometallics*, **2013**, *32*, 5668-5704.

[24] M. Alfonso, A. Espinosa Ferao, A. Tárraga, P. Molina, *Inorg. Chem.* **2015**, *54*, 7461-7473.

[25] Y. Hong, J. W. Y. Lam, B. Z. Tang, *Chem. Soc. Rev.* **2011**, *40*, 5361-5388.

[26] J. D. Luo, Z. L. Xie, J. W. Y. Lam, L. Cheng, H. Y. Chen, C. F. Qiu, H. S. Kwok, X. W. Zhan, Y. Q. Liu, D. B. Zhu, B. Z. Tang, *Chem. Comm*. **2001**, 1740-1741.

[27] J. Yang, Z. Chi, W. Zhu, B. Z. Tang, Z. Li, *Sci. China Chem.* **2019**, *62*, 1090-1098.

[28] M. Liu, Q. Wu, H. Shi, Z. An, W. Huang, *Acta Chimica Sinica*, **2018**, *76*, 246-258.

[29] C. Wang, B. Xu, M. Li, Z. Chi, Y. Xie, Q. Li, Z. Li, *Mater. Horizons* **2016**, *3*, 220-225.

[30] J. Yang, X. Gao, Z. Xie, Y. Gong, M. Fang, Q. Peng, Z. Chi, Z. Li, *Angew. Chem. Int. Ed.* **2017**, *56*, 15299-15303.

[31] Z. Hu, Y. Li, M. Kang, M. Islam, M. Chen, J. Zhang, Y. Xiao, X. Feng, C. Redshaw, M. Zhang, Q. Chen, S. Xie, J. W. Y. Lam, B. Z. Tang, *EcoMat* **2020**, *2*, e12024.

[32] S. Varughese, M. S. R. N. Kiran, U. Ramamurty, G. R. Desiraju, *Chem. Asian J.* **2012**, *7*, 2118-2125.

[33] T. Vy, R. Soklaski, Y. Liang, L. Yang, *Phys. Rev. B* **2014**, *89*, 235319.

[34] X. Wang, A. M. Jones, K. L. Seyler, T. Vy, Y. Jia, H. Zhao, H. Wang, L. Yang, X. Xu, F. Xia, *Nat. Nanotechnol.* **2015**, *10*, 517-521.

[35] G. Giri, E. Verploegen, S. C. B. Mannsfeld, S. Atahan-Evrenk, D. H. Kim, S. Y. Lee, H. A. Becerril, A. Aspuru-Guzik, M. F. Toney, Z. Bao, *Nature*, **2011**, *480*, 504-508.

[36] W. Wu, L. Wang, Y. Li, F. Zhang, L. Lin, S. Niu, D. Chenet, X. Zhang, Y. Hao, T. F. Heinz, J. Hone, Z. L. Wang, *Nature*, **2014**, *514*, 470–474.

[37] A. A. Shevyrin, A. G. Pogosov, A. K. Bakarov, A. A. Shklyaev, *Phys. Rev. Lett.* **2016**, *117***,** 017702.

[38] T. Jia, H.-R. Fuh, D. Chen, M. Abid, M. Abid, D. Zhang, A. B. Sarker, J. Cho, M. Choi, B. S. Chun, H. Xu, C. O. Coileain, H. Liu, C.-R. Chang, H.-C. Wu, *Adv. Electron. Mater.* **2018**, *4*, 1700447.

[39] Zhang, D.; Yang, Z.; Li, P.; Pang, M.; Xue, Q., *Nano Energy* **2019,** *65*, 103974.

[40] J.-L. Do, T. Friščić, *ACS Cent. Sci.* **2017**, *3*, 13-19.

[41] J. G. Hernández, C. Bolm, *J. Org. Chem.* **2017**, *82*, 4007-4019.

[42] A. Tuer, S. Krouglov, R. Cisek, D. Tokarz, V. Barzda, *J. Comput. Chem.* **2011**, *32*, 1128-1134.

[43] C. Adamo, V. Barone, *J. Chem. Phys.* **1999**, *110*, 6158-6170.

[44] I. Engeler, H. J. Hendricks Franssen, R. Müller, F. Stauffer, *J. Hydrol.* **2011**, *397*, 295-305.

[45] G. Kresse, J. Furthmuller, *Phys. Rev. B* **1996**, *54*, 11169.

[46] A. Aditya Prasad, K. Muthu, V. Meenatchi, M. Rajasekar, R. Agilandeshwari, K. Meena, J. Vijila Manonmoni, S. P. Meenakshisundaram, *Spectrochim. Acta A Mol. Biomol. Spectrosc.* **2015**, *140*, 311-327.

[47] C. Adamo, V. Barone. "Toward reliable density functional methods without adjustable parameters: The PBE0 model". In: *J. Chem. Phys.* **1999**, *110*, 6158–69 (cited on page 97)

[48] J. Zheng, X. Xu, D. G. Truhlar, *Theor. Chem. Acc.* **2011**, *128*, 295-305.

[49] Programs CrysAlis-CCD and -RED, Oxford Diffraction Ltd., Abingdon, UK (**2005**).

[50] Sheldrick, M.; SHELX-97 - Programs for crystal structure determination (SHELXS) and refinement (SHELXL), *Acta Cryst*. **2008**, *A64*, 112.

TOC

A novel ferrocene-based organic molecule crystal (Fc-Cz) that possesses anisotropic piezoelectric, optical, and mechanical properties. We demonstrate that the new crystal **Fc-Cz** can be utilized as an ultrasensitive piezoelectric material in fabricating strain sensors and energy harvesters.

Stimuli-responsive Materials from Ferrocene-based Organic Small Molecule for Wearable Sensors

Ling Li, Jianyu Zhang, Chenyi Yang, Le Huang, Jun Zhang, Jie Bai, Carl Redshaw, Xing Feng, Changyong Cao,* Nengjie Huo, Jingbo Li,* Ben Zhong Tang**